



**HAL**  
open science

# Old trees bloom new flowers, lysosome targeted near-infrared fluorescent probe for ratiometric sensing of hypobromous acid in vitro and in vivo based on Nile red skeleton

Wanqing Zhao, Pengyue Xu, Yixuan Ma, Yiming Song, Yihang Wang,  
Panpan Zhang, Bin Li, Yongmin Zhang, Jianli Li, Shaoping Wu

## ► To cite this version:

Wanqing Zhao, Pengyue Xu, Yixuan Ma, Yiming Song, Yihang Wang, et al.. Old trees bloom new flowers, lysosome targeted near-infrared fluorescent probe for ratiometric sensing of hypobromous acid in vitro and in vivo based on Nile red skeleton. *Bioorganic Chemistry*, 2024, 143, pp.107031. 10.1016/j.bioorg.2023.107031 . hal-04344732

**HAL Id: hal-04344732**

**<https://hal.sorbonne-universite.fr/hal-04344732>**

Submitted on 14 Dec 2023

**HAL** is a multi-disciplinary open access archive for the deposit and dissemination of scientific research documents, whether they are published or not. The documents may come from teaching and research institutions in France or abroad, or from public or private research centers.

L'archive ouverte pluridisciplinaire **HAL**, est destinée au dépôt et à la diffusion de documents scientifiques de niveau recherche, publiés ou non, émanant des établissements d'enseignement et de recherche français ou étrangers, des laboratoires publics ou privés.

1 **Old trees bloom new flowers, lysosome targeted near-infrared**  
2 **fluorescent probe for ratiometric sensing of hypobromous acid in**  
3 **vitro and in vivo based on Nile red skeleton**

4 Wanqing Zhao<sup>a</sup>, Pengyue Xu<sup>a</sup>, Yixuan Ma<sup>a</sup>, Yiming Song<sup>c,\*</sup>, Yihang Wang<sup>a</sup>, Panpan Zhang<sup>a</sup>, Bin  
5 Li<sup>a</sup>, Yongmin Zhang<sup>a,d</sup>, Jianli Li<sup>b</sup>, Shaoping Wu<sup>a,\*</sup>

6 <sup>a</sup> *Key Laboratory of Resource Biology and Biotechnology in Western China, Ministry of Education,*  
7 *Biomedicine Key Laboratory of Shaanxi Province, Northwest University, 229 Taibai Road,*  
8 *Xi'an, Shaanxi, 710069, P. R. China.*

9 <sup>b</sup> *Key Laboratory of Synthetic and Natural Functional Molecule Chemistry of the Ministry of*  
10 *Education, College of Chemistry and Materials Science, Northwest University, Xi'an, 710069, P.*  
11 *R. China.*

12 <sup>c</sup> *School of Chemical Engineering, Northwest University, 229 Taibai Road, Xi'an, Shaanxi, 710069,*  
13 *P. R. China.*

14 <sup>d</sup> *Sorbonne Université, CNRS, Institut Parisien de Chimie Moléculaire, UMR 8232, 4 place*  
15 *Jussieu, 75005, Paris, France.*

16 <sup>\*</sup> *Corresponding author.*

17 *E-mail addresses: [ymsong@nwu.edu.cn](mailto:ymsong@nwu.edu.cn) (Y. Song), [wushaoping@nwu.edu.cn](mailto:wushaoping@nwu.edu.cn) (S. Wu).*

18 **Abstract**

19 Hypobromous acid (HOBr), one of the significant reactive oxygen species (ROS)  
20 that acts as an important role in human immune system, however the increasing level  
21 of HOBr in human body can cause the disorder of eosinophils (EPO), leading to  
22 oxidative stress in organelles, and further causing a series of diseases. In this study, a  
23 ratiometric fluorescent probe **DMBP** based on Nile red skeleton was developed to  
24 detect HOBr specifically by the electrophilic substitution with HOBr. **DMBP** emits  
25 near-infrared (NIR) fluorescence at 653 nm, after reacting with HOBr, the emission  
26 wavelength of **DMBP** shifted blue and a new peak appeared at 520 nm, realizing a  
27 ratiometric examination of HOBr with a limit of detection of 89.00 nM. Based on its  
28 sensitive and specific response to HOBr, **DMBP** was applied in the visual imaging of

29 HOBr in HepG2 cells and zebrafish. Foremost, probe **DMBP** has excellent lysosome  
30 targeting ability and NIR emission reduced the background interference of biological  
31 tissues, providing a potential analytical tool to further investigate the role of HOBr in  
32 lysosome.

33

34 **Keywords:** Near infrared; Fluorescent probe; HOBr; Lysosome; Bioimaging

35

## 36 **1. Introduction**

37 Reactive oxygen species (ROS) are a class of oxygen-containing chemically  
38 reactive substances that are indispensable in cell signaling and maintenance of  
39 homeostasis in the body [1-3]. Hypobromic acid (HOBr) is one of the significant ROS  
40 which is generated by hydrogen peroxide and bromine ion catalyzed by eosinophils  
41 (EPO) in the human immune system [4-6]. HOBr possesses strong oxidizing and  
42 halogenating capabilities and therefore participates in a host of biological processes in  
43 the human defense system, like anti-inflammation, sterilization and resistance to  
44 pathogen invasion [7, 8]. However, the overexpression levels of HOBr in the body  
45 can lead to EPO disorders, which can result in oxidative stress in cellular organelles  
46 and further trigger a variety of physiopathological reactions, such as tissue injury,  
47 rheumatoid arthritis, cardiovascular diseases and cancers [9-11]. Therefore, the  
48 detection of HOBr level in vivo and vitro is crucial in clinical practice. In addition,  
49 lysosome is a main organelle of ROS production, and participates in the above  
50 processes [12, 13], hence it is essential to detect the level of HOBr in lysosome to

51 investigate its function in physiological processes[14]. However, there are relatively  
52 few methods to detect HOBr in lysosome, it is still a challenge to develop a novel  
53 method to monitor HOBr level in real time.

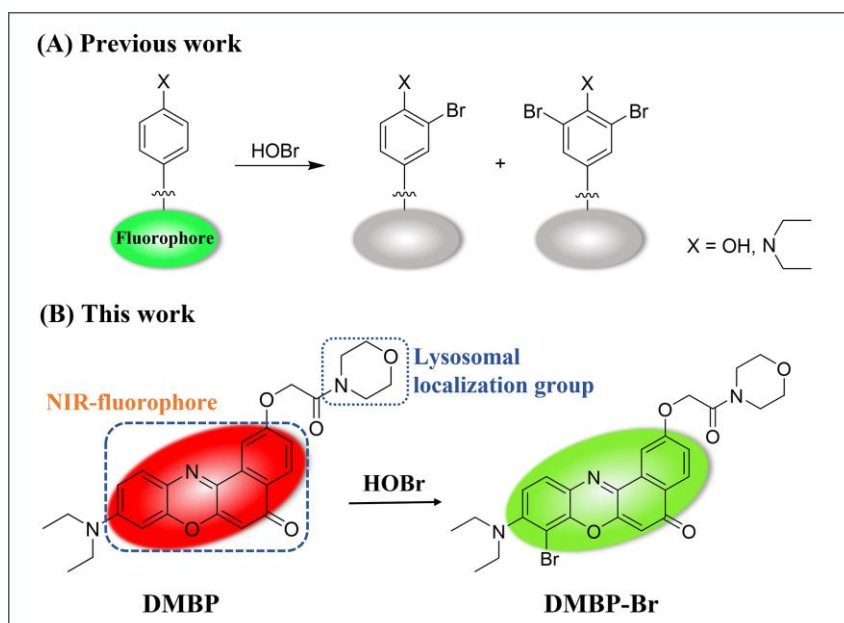
54 In recent years, fluorescent probe has rapidly entered the horizons of researchers  
55 due to its high sensitivity, good selectivity, real-time monitoring and non-invasive  
56 imaging, and has become an indispensable tool for monitoring small molecular  
57 substances in vivo and in vitro [15-20]. At present, the specific detection of HOBr  
58 based on fluorescent probe still faces great challenge for two reasons: (i) the low level  
59 of HOBr in vivo (2.00~100.00  $\mu\text{M}$ ). (ii) the oxidation capacity of HOBr is much  
60 weaker than HOCl and is seriously susceptible to interference by other ROS [21, 22].  
61 Therefore, there are relatively few fluorescent probes reported for the detection of  
62 HOBr. Han group firstly reported two redox fluorescent probes **mCy-TemOH** and  
63 **Cy-TemOH**, which can achieve ratiometric and quenching detection of HOBr,  
64 respectively, developed a new strategie for the detection of HOBr [23]. Kim group  
65 designed a BODIPY-based J-aggregating probe and utilized its electrophilic  
66 bromination to achieve the selective detection of HOBr generated by EPO [24], which  
67 was a pioneering work for the detection of HOBr by electrophilic substitution strategy.  
68 Overall, there are three detection mechanisms of fluorescent probe reported for HOBr  
69 detection [25]: (i) oxidation reaction caused by HOBr as a strong oxidant [26], (ii)  
70 HOBr-catalyzed coupling cyclization of amino groups with sulfur-methyl group [27],  
71 (iii) electrophilic substitution reaction of HOBr and small molecular compounds [28,  
72 29]. These sensing strategies were applied to design HOBr fluorescent probes based

73 on various fluorophores. In fact, in previous studies, the electrophilic halogenation of  
74 HOBr to electron-rich aromatic substrates showed stronger response than ClO<sup>-</sup> [30,  
75 31], and thus highly electrophilic properties of HOBr could be exploited to design its  
76 specific fluorescent probe.

77 Nevertheless, most of the HOBr fluorescent probes built on the aromatic  
78 bromination strategy were signal-off type owing to the intramolecular heavy atom  
79 impact [25] (Fig. 1A), and such probes are unattractive for the detection of HOBr,  
80 thus we are committed to finding a fluorophore with excellent properties to solve this  
81 problem. Fortunately, in this paper, we found that Nile red would not be quenched by  
82 HOBr, on the contrary, the bromination could cause a ratiometric change in  
83 fluorescence properties of Nile red to realize a ratiometric detection of HOBr. This  
84 discovery opens up a new idea for researchers to subsequently develop promising  
85 HOBr fluorescent probes.

86 In this work, we developed a NIR fluorescence probe **DMBP** built on Nile red  
87 skeleton (Fig. 1B). **DMBP** has an electron donor N, N-diethyl and receptor carbonyl  
88 that form ICT effect, which dominated the intense red fluorescence, and has a specific  
89 site for the detection of HOBr through electrophilic substitution reaction, which  
90 changed the optical properties of **DMBP**. Probe **DMBP** emits strong red fluorescence  
91 (653 nm) at prime, then the emission wavelength shifts to 520 nm after the addition of  
92 HOBr, achieving a ratiometric fluorescence response to HOBr. Moreover, probe  
93 **DMBP** has excellent selectivity and has been applied for visual imaging of HOBr in  
94 cells and zebrafish. Furthermore, **DMBP** can localize to lysosomes and realize the

95 ratio detection of HOBr in lysosomes.



96

97

**Fig. 1.** Design strategy of probe **DMBP**.

## 98 2. Experimental Section

### 99 2.1. Materials and Instruments

100 All solvents in the experiments were of analytical grade, water was treated by an  
101 ultra-water purification system, chemical reagents were purchased from Energy  
102 Chemical, and Lyso-Tracker Green was purchased from Beyotime Biotechnology.  
103 Fluorescence spectra were obtained by F-7000 fluorescence spectrophotometer and  
104 ultraviolet spectra were acquired from UV-1880 UV-Visible spectrophotometer.  
105 Confocal images were performed with a Leica TCS SP8 laser confocal microscope.  
106 The MS and NMR data were obtained by MicroTOF QII mass spectrometer and  
107 6001541ASP superconducting NMR instrument, respectively. Liquid chromatogram  
108 was obtained by LC-2030Plus high performance liquid chromatography system.

### 109 2.2. Synthesis of **DMBP**

110 Detailed synthesis method was described in Supporting Information (Scheme S1),

111 and the structure of **DMBP** was determined by MS (Fig. S4), <sup>1</sup>H NMR (Fig. S6) and  
112 <sup>13</sup>C NMR (Fig. S7).

### 113 *2.3. Spectral measurement*

114 Transferred 11.5 mg **DMBP** into a 25.00 mL volumetric bottle, and fixed it with  
115 DMSO to prepare the reserve solution, then 50.00 μL of **DMBP** (1.00 mmol/L), ion  
116 solutions, 1.00 mL of DMSO and 1.00 mL of PBS solution were added to the  
117 colorimetric tube in order, then fixed with deionized water to 5.00 mL. The excitation  
118 and emission slit widths of the fluorescence spectra were 5 nm and 10 nm respectively,  
119 and the voltage was 700 V. The ion solutions used in the experiments were prepared  
120 ready-to-use, and the detailed preparation methods were described in Supporting  
121 Information. All optical spectra were scanned at room temperature.

### 122 *2.4. Cell imaging experiment*

123 Cell imaging experiments were performed with HepG2 cells. Firstly, the  
124 cytotoxicity of probe **DMBP** was detected by MTT assay, and then the imaging  
125 experiment was carried out. Detailed experimental procedures were described in  
126 Supporting Information.

### 127 *2.5. Zebrafish imaging experiment*

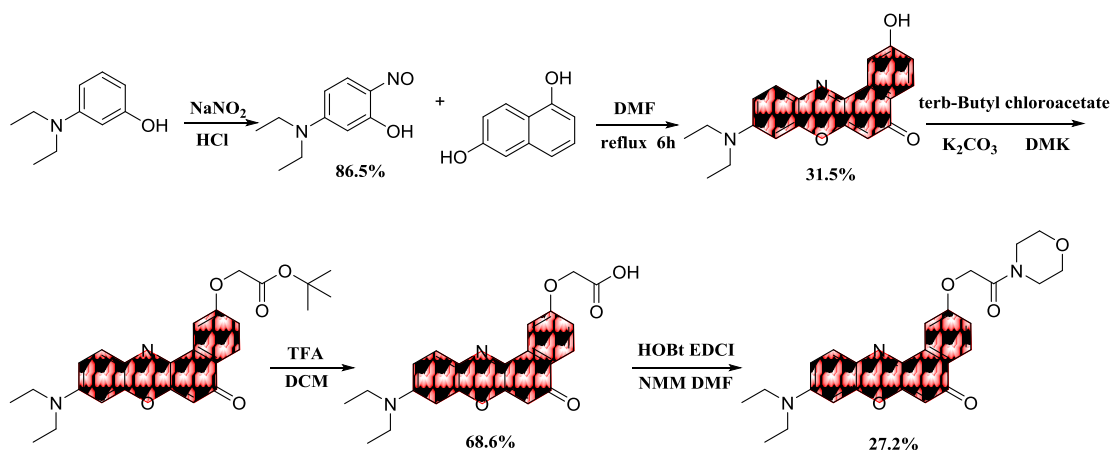
128 All zebrafish used in the experiments were in accordance with international  
129 ethical guidelines, and the three-day fertilized AB genotype zebrafish was selected as  
130 the experimental model. Detailed experimental procedures were described in  
131 Supporting Information.

## 132 **3. Results and Discussion**

### 133 3.1. Design of probe **DMBP**

134 We aimed to construct a ratiometric sensing platform to detect HOBr in  
135 lysosome. Redox reaction has been considered as a feasible strategy for detecting  
136 ROS, however, it is difficult to be adopted to detect HOBr because HOBr has similar  
137 character, weaker oxidation capacity and lower concentration compared to  $\text{ClO}^-$  in  
138 vivo [32, 33], which may cause non-negligible influence. Literatures reported that  
139 electrophilic halogenation of electron-rich aromatic substrates or olefins by HOBr  
140 shows stronger reactivity than  $\text{ClO}^-$ . Mainly because  $\text{Br}^-$  is formed as an intermediate  
141 in these reactions, compared with  $\text{Cl}^-$ ,  $\text{Br}^-$  has lower electronegativity and higher  
142 polarizability, making it more receptive to positive charges, and thus HOBr exhibits  
143 higher electrophilicity [24, 34]. Therefore, the high electrophilic property of HOBr  
144 can be used to design its specific fluorescent probe. As a classical NIR fluorescent dye,  
145 Nile red has excellent properties such as low background interference, deep tissue  
146 penetration and good photostability [35-37], and most importantly, the aromatic ring  
147 contained in Nile red can react with HOBr through electrophilic substitution, which is  
148 an ideal fluorophore for the design of HOBr fluorescent probe. In our design strategy  
149 (Fig. 1B), Nile red scaffold is used as the fluorophore, the morpholine ring as the  
150 lysosomal localization group [38, 39], and the aromatic ring in molecule can react  
151 with HOBr to generate brominated products by electrophilic substitution, which can  
152 inhibit the intramolecular charge transfer (ICT) of probe **DMBP** (the synthesis route  
153 was shown in Scheme 1, yield: 27.2%), thus affecting the spectral properties of probe  
154 **DMBP** to produce a ratiometric fluorescence response.



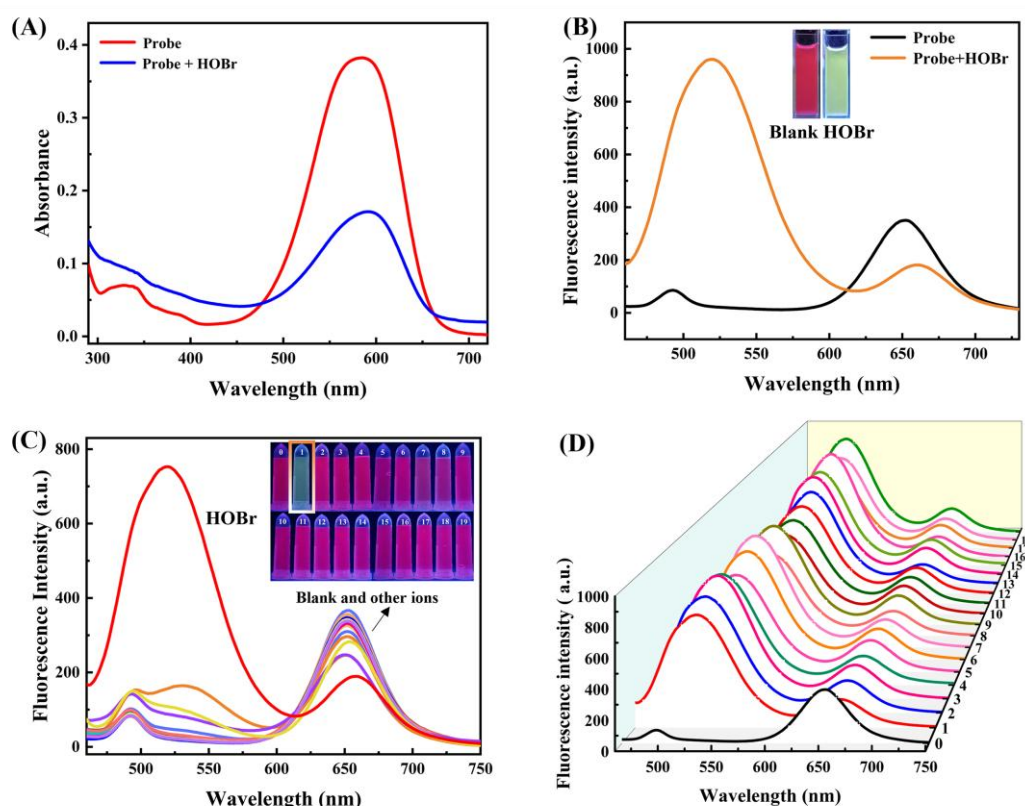


Scheme 1. Synthetic route of probe **DMBP**.

### 3.2. Spectral properties of **DMBP**

Firstly, the molar absorption coefficient, fluorescence quantum yield and other related spectral properties of probe **DMBP** were measured in different organic solvents (Table S3). **DMBP** has NIR emission (653 nm) and high fluorescence quantum yield up to 30.00%, with deep tissue penetration and low background, which demonstrated its broad prospect in biological imaging. Then we examined the absorption and emission spectra of **DMBP** before and after the reaction with HOBr. The absorption and emission peaks of **DMBP** were at 580 nm and 653 nm respectively (Fig. 2A, 2B). The absorption peak at 580 nm was decreased significantly after the addition of HOBr, accompanied by an increasing peak at 420 nm (Fig. 2A). Meanwhile, the ratio changes appeared in the fluorescence spectra, the emission peak at 653 nm decreased together with an arising emission peak at 520 nm after the reaction between **DMBP** and HOBr (Fig. 2B). Selectivity and competition studies were used to demonstrate the specificity of **DMBP** to HOBr, the above results showed that other biologically relevant analytes, common anions and cations in humans would not cause ratiometric response of **DMBP** or influence the detection of

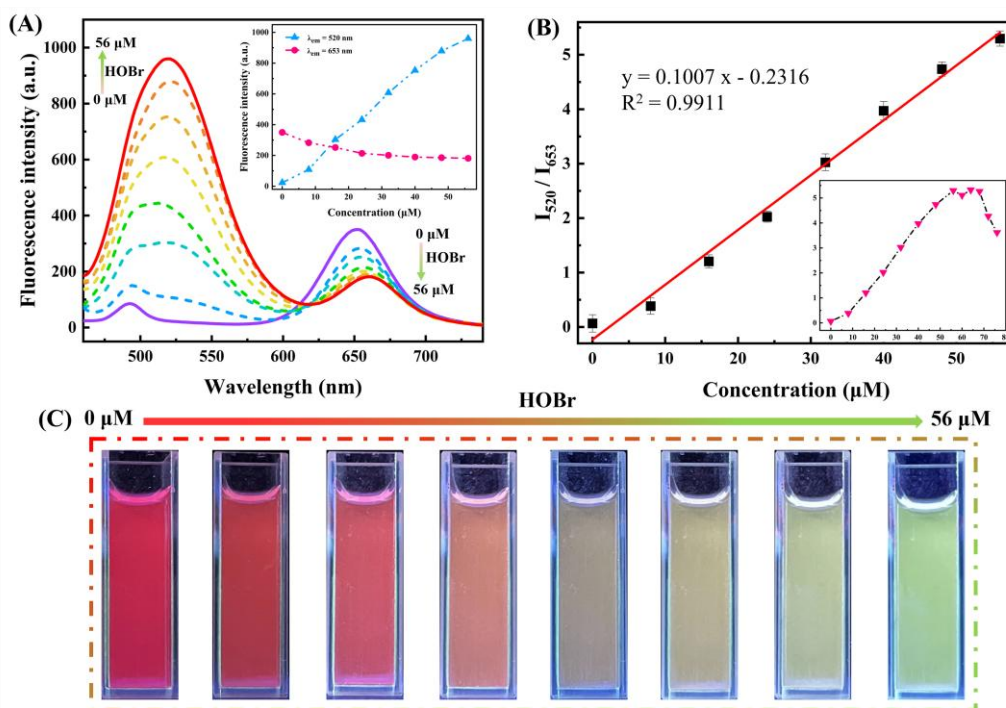
173 HOBr (Fig. 2C, 1D), indicating that **DMBP** has excellent selectivity for HOBr and  
 174 powerful anti-interference ability.



175  
 176 **Fig. 2.** (A) UV absorption spectra before and after the reaction of **DMBP** with HOBr. (B)  
 177 Fluorescence emission spectra before and after the reaction of **DMBP** with HOBr. (C)  
 178 Fluorescence spectra of **DMBP** (10.00  $\mu\text{M}$ ) upon addition of 40.0  $\mu\text{M}$  19 kinds of ions (0: blank;  
 179 1: HOBr; 2:  $\text{H}_2\text{O}_2$ ; 3:  $\text{ClO}^-$ ; 4: NO; 5:  $\text{ROO}^-$ ; 6:  $\cdot\text{OH}$ ; 7:  $^1\text{O}_2$ ; 8:  $\text{ONOO}^-$ ; 9: *t*-BuOOH; 10: GSH; 11:  
 180 Cys; 12: Hcy; 13:  $\text{S}^{2-}$ ; 14:  $\text{K}^+$ ; 15:  $\text{Ca}^{2+}$ ; 16:  $\text{Mg}^{2+}$ ; 17:  $\text{Fe}^{2+}$ ; 18:  $\text{Br}^-$ ; 19:  $\text{NO}_2^-$ ). (D) Competitive  
 181 fluorescence spectra of **DMBP** (10.0  $\mu\text{M}$ ) with HOBr and other biologically relevant species.  $\lambda_{\text{ex}}$   
 182 = 420 nm. Insets in (B): Pictures of before and after the reaction of **DMBP** with HOBr under 365  
 183 nm excitation. Insets in (C): Pictures of **DMBP** upon treatment with various ions under 365 nm  
 184 excitation.

185 The impact of HOBr concentration on the spectral properties of **DMBP** was next  
 186 investigated. Fig. 3A showed the variation trend, the increasing concentration of  
 187 HOBr caused rising fluorescence intensity at 520 nm (green) and reducing at 653 nm  
 188 (red) of **DMBP**. The ratio of green to red fluorescence intensity of **DMBP** was  
 189 proportional to HOBr (0~56.00  $\mu\text{M}$ ), whose correlation index reached 0.9911 and  
 190 possessed a lower Limit of Detection (LOD) of 89.00 nM (Fig. 3B). The above

191 experimental results indicated that **DMBP** could response to different concentrations  
 192 of HOBr selectively and showed a ratiometric variation, rendering **DMBP** an ideal  
 193 probe for the sensitive and accurate detection of HOBr.



194  
 195 **Fig. 3.** (A) Fluorescence emission curves of **DMBP** (10.00  $\mu\text{M}$ ) with added HOBr (0~56.00  $\mu\text{M}$ )  
 196 (pH 7.4, 20% DMSO); slit widths: 5/10 nm; operating voltage: 700 V;  $\lambda_{\text{ex}} = 420 \text{ nm}$ . (B) Linear  
 197 correlation of (A). (C) Fluorescence photos ( $\lambda_{\text{ex}} = 365 \text{ nm}$ ) of probe **DMBP** after reacting with  
 198 HOBr (0  $\mu\text{M}$ , 8.00  $\mu\text{M}$ , 16.00  $\mu\text{M}$ , 24.00  $\mu\text{M}$ , 32.00  $\mu\text{M}$ , 40.00  $\mu\text{M}$ , 48.00  $\mu\text{M}$ , 56.00  $\mu\text{M}$ ). Inset in  
 199 (A): Fluorescence intensity changes at 653 nm and 520 nm. Inset in (B): Fluorescence intensity  
 200 ratio ( $I_{520}/I_{653}$ ) with added HOBr (0~76.00  $\mu\text{M}$ ).

201 We also explored the effects of time and pH to examine the dynamics and pH  
 202 tolerance of **DMBP** and its response to HOBr (Fig. S12). Firstly, the kinetic properties  
 203 between **DMBP** and HOBr were investigated (Fig. S12A), after the addition of HOBr,  
 204 the fluorescence signal ratio ( $I_{520}/I_{653}$ ) of **DMBP** enhanced 40-fold within 1 min and  
 205 reached equilibrium within 10 mins. Next, we evaluated the pH tolerance of **DMBP**  
 206 and the reaction system, as shown in Fig. S12B, after the addition of 40.0  $\mu\text{M}$  of  
 207 HOBr, probe **DMBP** showed stable fluorescence emission of  $I_{520}/I_{653}$  under pH 3~12

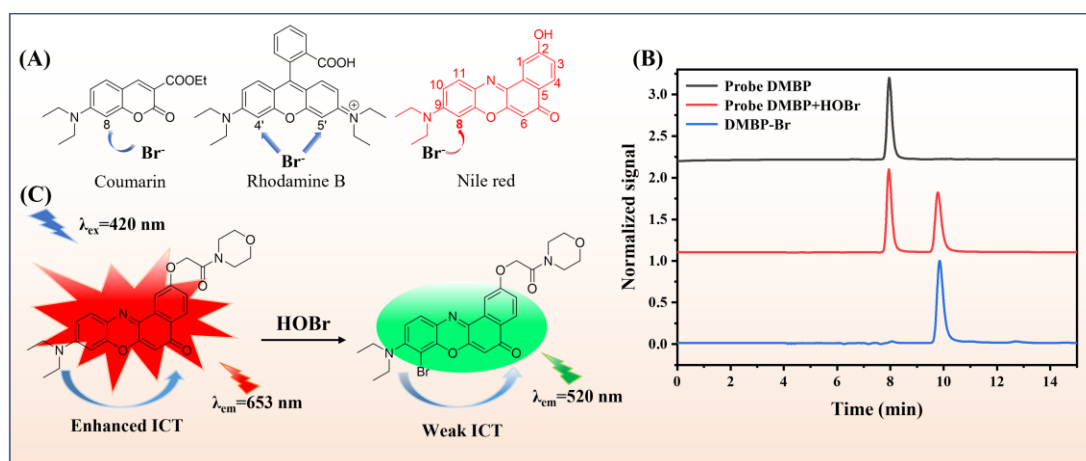
208 that contained physiological conditions. The above results indicated that **DMBP** is an  
209 excellently sensitive and stable fluorescent probe to detect HOBr.

### 210 3.3. Validation of reaction mechanism

211 The electron donor *N, N*-diethyl and acceptor carbonyl groups exist in **DMBP**  
212 forming the ICT effect, and producing intense red fluorescence. According to the  
213 changes of fluorescence emission, the adding of HOBr caused significant reduction of  
214 intensity at 653 nm and increased at 520 nm, resulting in a blue shift of fluorescence  
215 spectra, which may be attributed to the bromine substituent reduced the electron  
216 density of the oxygen heterocycle.

217 It was reported that HOBr could attack the 5-position of coumarin and the 4'(5')  
218 position of rhodamine B to generate brominated products, and the 8-position of  
219 **DMBP** had similar substituents in the adjacent position with them [28]. Therefore, it  
220 was speculated that the electrophilic substitution of HOBr occurred at the 8-position  
221 of **DMBP** (Fig. 4A). After the electrophilic substitution reaction between **DMBP** and  
222 HOBr, the bromine replaced the hydrogen at the 8-position of probe, which  
223 effectively inhibited the ICT process, and triggered a blue shift of emission  
224 wavelength to produce a ratiometric fluorescence signal. For further confirmation of  
225 the mechanism, we subjected the reaction product to mass spectrometry and liquid  
226 phase analysis. Probe **DMBP** was dissolved in methanol at a final concentration of  
227 10.00  $\mu\text{M}$ , then detected with an injection volume of 10.00  $\mu\text{L}$ . The eluent was  
228 methanol at a flow rate of 1  $\text{mL}\cdot\text{min}^{-1}$ , probe **DMBP** (10.00  $\mu\text{M}$ ) was treated with  
229 HOBr (50.00  $\mu\text{M}$ ) for 10 min, signals were collected at 420 nm and 580 nm. As

230 shown in Fig. 4B, probe **DMBP** had a chromatographic peak at 7.9 min after isocratic  
 231 elution with 85% methanol, and a new peak at 9.8 min appeared after the reaction  
 232 with HOBr, which demonstrated the generation of new product. To further determine  
 233 the structure of the new product, we purified and subjected it to mass spectrometry,  
 234 the measured mass spectral peak was 562.0947 (Fig. S5), which was consistent with  
 235 the calculated value of **DMBP-Br** as 562.0954, providing a proof of the generation of  
 236 **DMBP-Br**. Subsequently, the synthesized **DMBP-Br** was subjected to liquid phase  
 237 analysis, and the peak position was consistent with the reaction product,  
 238 demonstrating that the probe reacted with HOBr to form **DMBP-Br**.



239 **Fig. 4.** (A) Prediction of reaction sites between probe **DMBP** and HOBr. (B) Liquid phase spectra  
 240 before and after the reaction with HOBr. (C) Reaction mechanism between probe **DMBP** and  
 241 HOBr.  
 242 HOBr.

#### 243 3.4. Fluorescence imaging of HOBr in HepG2 cells

244 Before cell imaging, the toxicity of **DMBP** to HepG2 cells was assessed by MTT  
 245 assay firstly (Fig. S10), more than 80% of HepG2 cells survived when the  
 246 concentration of **DMBP** reached 12.50  $\mu\text{M}$ , indicating that probe **DMBP** had lower  
 247 cytotoxicity and was available for cell imaging.

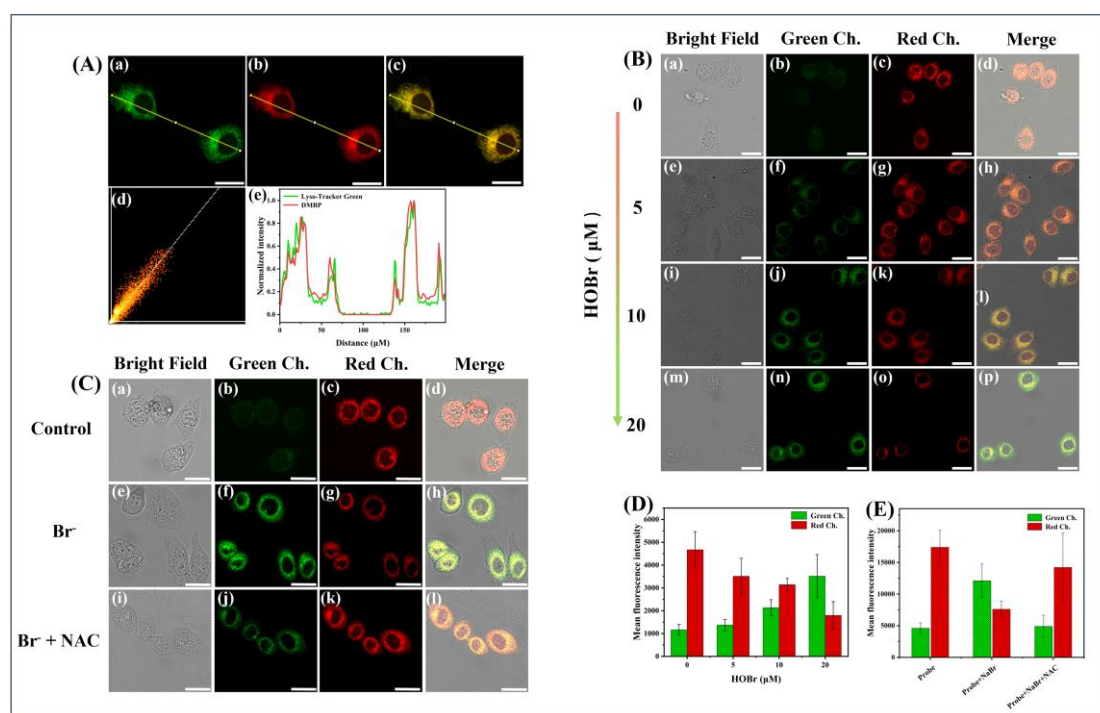
248 There are many reactive oxygen species involved in reactions inside lysosomes,

249 so it is interesting to study the reactive oxygen species inside lysosomes. We attached  
250 a lysosomal localization motif to the designed probe and determined the localization  
251 of **DMBP** in the lysosome by co-localization imaging experiments. As shown in Fig.  
252 5A, after co-incubation with Lyso-Tracker Green (a commercially available lysosomal  
253 green fluorescent probe) and **DMBP** with HepG2 cells for 3 min, the red fluorescence  
254 collected by the probe highly overlapped with the green fluorescence of Lyso-Tracker  
255 Green. In addition, the cross-sectional fluorescence intensity distributions of **DMBP**  
256 and Lyso-Tracker Green in the cells were essentially identical (Pearson coefficient  
257 was 0.97), indicating that probe **DMBP** could be localized in lysosomes.

258 Then the response of **DMBP** to exogenous HOBr in living cells was investigated.  
259 The green and red channels were set up for simultaneous detection, an obvious  
260 fluorescence signal could be observed in the red channel but almost none in the green  
261 channel when **DMBP** was incubated with cells (Fig. 5B). However, after the  
262 incubation of HOBr, the fluorescence of the red channel decreased and that of the  
263 green channel was significantly enhanced, indicating that **DMBP** could be used to  
264 detect exogenous HOBr. In addition, the fluorescence intensity changes of two  
265 channels were positively correlated with the concentration of HOBr, which suggested  
266 that **DMBP** could realize visualization of exogenous HOBr in living cells.

267 Some abnormal activities in the organism can change the concentration of HOBr  
268 in the lysosome, therefore, observing the change of endogenous HOBr is beneficial to  
269 determine the role it plays in the lysosome. Fig. 5C shows the fluorescence imaging  
270 experiment of **DMBP** on endogenous HOBr. HepG2 cells treated with **DMBP** only

271 showed red fluorescence, after the stimulation of NaBr to produce HOBr in cells, the  
 272 fluorescence at red channel was weakened, while the fluorescence at the green  
 273 channel was significantly enhanced, and this trend was correlated with the  
 274 concentration of NaBr. Subsequently, the added reagent NAC (a scavenger of HOBr)  
 275 decreased the green fluorescence signal significantly, which proved that the change of  
 276 fluorescence signal at the green channel was caused by the generation of HOBr. In  
 277 summary, probe **DMBP** can monitor the fluctuation of exogenous and endogenous  
 278 HOBr in HepG2 cells in real time and is expected to be used to examine the role of  
 279 HOBr in lysosomes.



280  
 281 **Fig. 5.** (A) Co-localization images of Lysosomes. (a) Lyso-Tracker Green (1.00 μM), (b) **DMBP**  
 282 (5.00 μM), (c) merged image. Green channel was acquired at 500~600 nm,  $\lambda_{ex} = 488$  nm, red  
 283 channel was acquired at 610~750 nm,  $\lambda_{ex} = 552$  nm. (d) Co-localization scatter plot of (a). (e)  
 284 Cross section intensity of (a). (B) Confocal fluorescence images of HepG2 cells with **DMBP** (5.00  
 285 μM) and exogenous HOBr (0 μM, 5.00 μM, 10.00 μM, 20.00 μM). (C) Confocal fluorescence  
 286 images of HepG2 cells with **DMBP** (5.00 μM) and endogenous HOBr. (a-d) control; (e-h) NaBr  
 287 (20.00 μM); (i-l) NaBr (20.00 μM) and NAC (250.00 μM). (D) Digitization fluorescence intensity  
 288 of each group of cells in (B). (E) Digitization fluorescence intensity of each group of cells in (C).  
 289 Green channel was acquired at 480~600 nm,  $\lambda_{ex} = 405$  nm, red channel was acquired at 610~750

290 nm,  $\lambda_{\text{ex}} = 552$  nm, Scale bar: 25  $\mu\text{m}$ .

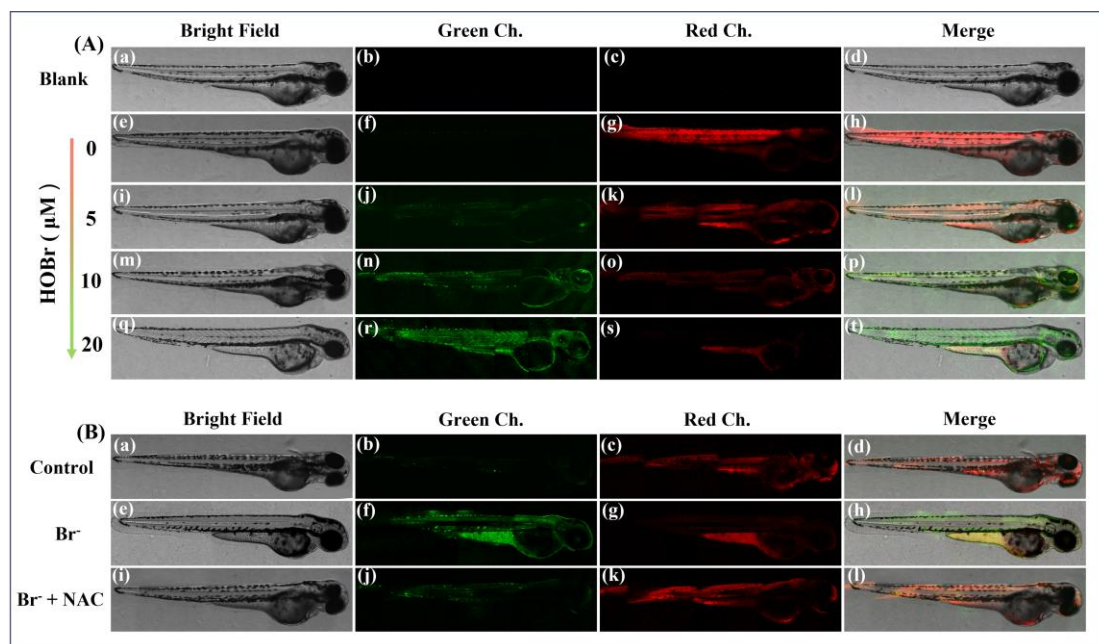
### 291 3.5. Fluorescence imaging of HOBr in zebrafish

292 Given the relatively promising detection ability of probe **DMBP** in cells, we  
293 further explored its application in zebrafish. Using three-day zebrafish as animal  
294 model, we first investigated the fluorescence signal in zebrafish before and after the  
295 addition of exogenous HOBr. As shown in Fig. 6A, after incubation of **DMBP** with  
296 zebrafish alone, there was a clear fluorescence signal at red channel but almost not at  
297 green channel. Conversely, the zebrafish incubated with **DMBP** and different  
298 concentrations of HOBr showed gradually enhanced fluorescence signal at the green  
299 channel and decreased at the red channel. The above results demonstrate that probe  
300 **DMBP** can detect exogenous HOBr in animal models, further indicating its promising  
301 application for in vivo imaging.

302 EPO can catalyze a reaction to produce HOBr, making the concentration of  
303 HOBr correlate with EPO activity, which is associated with inflammation and tissue  
304 damage in vivo; therefore, detection of endogenous HOBr concentration is expected  
305 to enable monitoring of EPO activity for early diagnosis of diseases. Based on this  
306 information, we imaged endogenous HOBr (induced by NaBr) in zebrafish using  
307 probe **DMBP**. Enhanced green fluorescence and attenuated red fluorescence were  
308 observed in zebrafish treated with NaBr. To demonstrate that the change in  
309 fluorescence was caused by HOBr, we also made a control experiment using reagent  
310 NAC to eliminate the HOBr induced by NaBr, and as shown in the Fig. 6B, the green  
311 fluorescence was significantly weakened, demonstrating that the change in  
312 fluorescence of the green channel was caused by HOBr. The above experiments



313 manifested that probe **DMBP** is capable of detecting endogenous HOBr in organisms,  
 314 and is expected to be used for early diagnosis of diseases.



315 **Fig. 6.** (A) Confocal fluorescence images of zebrafish with probe **DMBP** (5.0 μM) and  
 316 exogenous HOBr (0 μM, 5.00 μM, 10.00 μM, 20.00 μM). (B) Confocal fluorescence images of  
 317 **DMBP** (5.00 μM) and endogenous HOBr in zebrafish. (a-d) control; (e-h) NaBr (20.00 μM); (i-l)  
 318 NaBr (20.00 μM) and NAC (250.00 μM). Green channel was acquired at 480~600 nm,  $\lambda_{ex}$  =405  
 319 nm, red channel was acquired at 610~750 nm,  $\lambda_{ex}$  =552 nm.

#### 321 4. Conclusion

322 In summary, we designed and synthesized a lysosome-targeted NIR fluorescent  
 323 probe **DMBP** based on the Nile red skeleton. The experiment result shows that HOBr  
 324 can react with the probe via electrophilic substitution, resulting in an increasing  
 325 emission peak at 520 nm, which produced a ratiometric signal change from red to  
 326 green depending on the change of ICT process. **DMBP** exhibits high selectivity and  
 327 sensitivity to HOBr and can rapidly distinguish other ROS. **DMBP** also has good  
 328 biocompatibility and cell permeability that had been successfully used for exogenous  
 329 and endogenous HOBr imaging in HepG2 cells and zebrafish. More importantly, as  
 330 the first NIR fluorescent probe can simultaneously localize lysosomes and achieve

331 ratiometric detection of HOBr, we believe that probe **DMBP** is a potential tool for the  
332 diagnosis of HOBr-related diseases in lysosomes.

### 333 **CrediT authorship contribution statement**

334 **Wanqing Zhao:** Conceptualization, Methodology, Data Curation, Writing -  
335 Original Draft, Writing-Review & Editing. **Pengyue Xu:** Methodology, Data Curation,  
336 Writing-Review & Editing. **Yixuan Ma:** Validation, Data Curation. **Yiming Song:**  
337 Supervision, Project administration, Conceptualization, Methodology, Writing-review  
338 & editing. **Yihang Wang:** Methodology, Investigation, Data Curation, Formal  
339 analysis. **Panpan Zhang:** Investigation, Data Curation, Formal analysis. **Bin Li:**  
340 Investigation, Data Curation, Formal analysis. **Yongmin Zhang:** Conceptualization,  
341 Writing-review & editing. **Jianli Li:** Data Curation, Conceptualization. **Shaoping Wu:**  
342 Supervision, Project administration, Conceptualization, Methodology, Writing-review  
343 & editing.

### 344 **Declaration of Competing Interest**

345 The authors declare that they have no known competing financial interests or  
346 personal relationships that could have appeared to influence the work reported in this  
347 paper.

### 348 **Data availability**

349 Data will be made available on request.

### 350 **Acknowledgements**

351 The authors thank the National Natural Science Foundation of China (No.  
352 21572177), the Key Research and Development Program of Shaanxi Province (No.

353 2021ZDLSF03-03), Biomedicine Key Laboratory of Shaanxi Province (No.  
354 2018SZS41).

### 355 **Appendix A. Supplementary data**

356 Supplementary data to this article can be found online at <https://xxx>

### 357 **References**

- 358 [1] S. Antonucci, F.D. Lisa, N. Kaludercic, Mitochondrial reactive oxygen species in physiology  
359 and disease, *Cell Calcium*. 94 (2021), 102344.
- 360 [2] Y. Dai, Y. Ding, L. Li, Nanozymes for regulation of reactive oxygen species and disease  
361 therapy, *Chin Chem Lett*. 32 (9) (2021) 2715-2728.
- 362 [3] X.-M. Cheng, Y.-Y. Hu, T. Yang, N. Wu, X.-N. Wang, Reactive oxygen species and oxidative  
363 stress in vascular-related diseases, *Oxid. Med. Cell. Longev*. 2022 (2022), 7906091.
- 364 [4] S.J. Weiss, S.T. Test, C.M. Eckmann, D. Roos, S. Regiani, Brominating oxidants generated by  
365 human eosinophils, *Science*. 234 (4773) (1986), 200-203.
- 366 [5] J. Wang, A. Slungaard, Role of eosinophil peroxidase in host defense and disease pathology,  
367 *Arch. Biochem*. 445 (2) (2006) 256-260.
- 368 [6] T. Suzuki, M. Kumagai, M. Furusawa, Effects of urea on the reactions of nucleosides with  
369 hypobromous acid, *Chem. Pharm. Bull*. 67 (7) (2019) 707-712.
- 370 [7] A.S. McCall, Christopher F. Cummings, G. Bhave, R. Vanacore, A. Page-McCaw, B.G.  
371 Hudson, Bromine is an essential trace element for assembly of collagen IV scaffolds in tissue  
372 development and architecture, *Cell*. 157 (6) (2014) 1380-1392.
- 373 [8] T. Suzuki, A. Okuyama, Reactions of rebamipide with hypobromous acid, *Chem. Pharm. Bull*.  
374 67 (10) (2019) 1164-1167.
- 375 [9] Y.W. Yap, M. Whiteman, N.S. Cheung, Chlorinative stress: An under appreciated mediator of  
376 neurodegeneration?, *Cell. Signal*. 19 (2) (2007) 219-228.
- 377 [10] C. Gorrini, I.S. Harris, T.W. Mak, Modulation of oxidative stress as an anticancer strategy,  
378 *Nat. Rev. Drug Discov*. 12 (12) (2013) 931-947.
- 379 [11] K.L. Brown, C. Darris, K.L. Rose, O.A. Sanchez, H. Madu, J. Avance, N. Brooks, M.-Z.  
380 Zhang, A. Fogo, R. Harris, B.G. Hudson, P. Voziyan, Hypohalous acids contribute to renal

381 extracellular matrix damage in experimental diabetes, *Diabetes*. 64 (6) (2015) 2242-2253.

382 [12] T. Kurz, A. Terman, B. Gustafsson, U.T. Brunk, Lysosomes and oxidative stress in aging and  
383 apoptosis, *Biochim Biophys Acta Gen Subj*. 1780 (11) (2008) 1291-1303.

384 [13] Z. Dong, W. Liang, Y. Dong, H. Ren, Y. Wang, Water-soluble dual lysosome/mitochondria-  
385 targeted fluorescent probe for detection of SO<sub>2</sub> in water, food, herb, and live cells, *Bioorg.*  
386 *Chem*. 129 (2022), 106189.

387 [14] X. Duan, Q. Tong, C. Fu, L. Chen, Lysosome-targeted fluorescent probes: design mechanism  
388 and biological applications, *Bioorg. Chem*. 140 (2023), 106832.

389 [15] L. Guan, W. Hu, H. Zuo, H. Sun, Y. Ai, M.-H. He, C. Ma, M. Ding, Q. Liang, An NIR  
390 fluorescent/photoacoustic dual-mode probe of NADPH for tumor imaging, *Chem. Commun*.  
391 59 (12) (2023) 1617-1620.

392 [16] X. Li, Q. Feng, L. Qu, T. Zhao, X. Li, T. Bai, S. Sun, S. Wu, Y. Zhang, J. Li, A water-soluble  
393 and incubate-free fluorescent environment-sensitive probe for ultrafast visualization of  
394 protein thiols within living cells, *Anal Chim Acta*. 1126 (2020) 72-81.

395 [17] S. Zhang, B. Li, J. Zhou, J. Shi, Z. He, Y. Zhao, Y. Li, Y. Shen, Y. Zhang, S. Wu, Kill three  
396 birds with one stone: mitochondria-localized tea saponin derived carbon dots with AIE  
397 properties for stable detection of HSA and extremely acidic pH, *Food Chem*. 405 (2023),  
398 134865.

399 [18] Q. Feng, Y. Song, Y. Ma, Y. Deng, P. Xu, K. Sheng, Y. Zhang, J. Li, S. Wu, Molecular  
400 engineering of benzenesulfonyl analogs for visual hydrogen polysulfide fluorescent probes  
401 based on Nile red skeleton, *Spectrochim. Acta A Mol. Biomol. Spectrosc*. 296 (2023),  
402 122658.

403 [19] H. Zhu, M. Liu, C. Liu, X. Li, K. Wang, M. Yu, W. Sheng, B. Zhu, A reversible and  
404 ratiometric fluorescent probe based on rhodol derivative with an ESIPT unit for monitoring  
405 copper ion content and in situ evaluation of related drugs in cells, *Bioorg. Chem*. 139 (2023),  
406 106733.

407 [20] W.-J. Bi, Z.-X. Lan, X.-C. Wang, Y.-X. Cheng, J.-B. Jiang, Design and synthesis of  
408 photoaffinity-based probes for labeling  $\beta$ -glucuronidase, *Bioorg. Chem*. 141 (2023), 106909.

409 [21] K. Xu, H. Chen, J. Tian, B. Ding, Y. Xie, M. Qiang, B. Tang, A near-infrared reversible

410 fluorescent probe for peroxynitrite and imaging of redox cycles in living cells, *Chem.*  
411 *Commun.* 47 (33) (2011) 9468-9470.

412 [22] B. Wang, P. Li, F. Yu, J. Chen, Z. Qu, K. Han, A near-infrared reversible and ratiometric  
413 fluorescent probe based on Se-BODIPY for the redox cycle mediated by hypobromous acid  
414 and hydrogen sulfide in living cells, *Chem. Commun.* 49 (51) (2013) 5790-5792.

415 [23] F. Yu, P. Song, P. Li, B. Wang, K. Han, Development of reversible fluorescence probes based  
416 on redox oxoammonium cation for hypobromous acid detection in living cells, *Chem.*  
417 *Commun.* 48 (62) (2012) 7735-7737.

418 [24] T.I. Kim, B. Hwang, B. Lee, J. Bae, Y. Kim, Selective monitoring and imaging of eosinophil  
419 peroxidase activity with a J-aggregating probe, *J. Am. Chem. Soc.* 140 (37) (2018) 11771-  
420 11776.

421 [25] D. Zhang, X. Yang, T. Wang, X. Ji, X. Wu, Advances in organic fluorescent probes for  
422 bromide ions, hypobromous acid and related eosinophil peroxidase-A review, *Anal. Chim.*  
423 *Acta.* 1244 (2023), 340626.

424 [26] X. Huo, X. Wang, R. Yang, Z. Li, Y. Sun, L. Qu, H. Zeng, A novel fluorescent probe for  
425 highly selective and sensitive detection of hypobromous acid in arthritis model mice, *Sens*  
426 *Actuators B Chem.* 315 (2020), 128125.

427 [27] P. Jia, D. Liu, Z. Zhuang, L. Qu, C. Liu, Y. Zhang, Z. Li, H. Zhu, Y. Yu, X. Zhang, W. Sheng,  
428 B. Zhu, A highly selective ratiometric fluorescence probe for bioimaging of hypobromous  
429 acid in living cells and zebrafish, *Sens Actuators B Chem.* 320 (2020), 128583.

430 [28] L. Wu, Y. Shi, H. Yu, J. Zhang, Z. Li, X.-F. Yang, Bromination-induced spirocyclization of  
431 rhodamine dyes affording a FRET-based ratiometric fluorescent probe for visualization of  
432 hypobromous acid (HOBr) in live cells and zebrafish, *Sens Actuators B Chem.* 337 (2021),  
433 129790.

434 [29] H. Zhu, P. Jia, X. Wang, Y. Tian, C. Liu, X. Li, K. Wang, P. Li, B. Zhu, B. Tang, In situ  
435 observation of lysosomal hypobromous acid fluctuations in the brain of mice with depression  
436 phenotypes by two-photon fluorescence imaging, *Anal. Chem.* 94 (34) (2022) 11783-11790.

437 [30] D.I. Pattison, M.J. Davies, Kinetic Analysis of the reactions of hypobromous acid with  
438 protein components: implications for cellular damage and use of 3-bromotyrosine as a

439 marker of oxidative stress, *Biochemistry*. 43 (16) (2004) 4799-4809.

440 [31] V.F. Ximenes, N.H. Morgon, A.R. de Souza, Hypobromous acid, a powerful endogenous  
441 electrophile: experimental and theoretical studies, *J. Inorg. Biochem.* 146 (2015) 61-68.

442 [32] S.-R. Liu, S.-P. Wu, Hypochlorous acid turn-on fluorescent probe based on oxidation of  
443 diphenyl selenide, *Org. Lett.* 15 (4) (2013) 878-881.

444 [33] S.T. Manjare, S. Kim, W.D. Heo, D.G. Churchill, Selective and sensitive superoxide detection  
445 with a new diselenide-based molecular probe in living breast cancer cells, *Org. Lett.* 16 (2)  
446 (2014) 410-412.

447 [34] C.L. Hawkins, M.J. Davies, The role of aromatic amino acid oxidation, protein unfolding, and  
448 aggregation in the hypobromous acid-induced inactivation of trypsin inhibitor and lysozyme,  
449 *Chem. Res. Toxicol.* 18 (11) (2005) 1669-1677.

450 [35] Z. Peng, B. Zhang, Nanobubble labeling and imaging with a solvatochromic fluorophore Nile  
451 red, *Anal. Chem.* 93 (46) (2021) 15315-15322.

452 [36] R. Sun, W. Wan, W. Jin, Y. Bai, Q. Xia, M. Wang, Y. Huang, L. Zeng, J. Sun, C. Peng, B.  
453 Jing, Y. Liu, Derivatizing Nile red fluorophores to quantify the heterogeneous polarity upon  
454 protein aggregation in the cell, *Chem. Commun.* 58 (35) (2022) 5407-5410.

455 [37] H. Sun, Y. Du, X. Chen, H. Jiang, Y. Li, L. Shen, Design, synthesis, and evaluation of Nile red  
456 analogs for myelin imaging as near-infrared fluorescence probe, *Dyes Pigm.* 208 (2022),  
457 110804.

458 [38] X. Wang, L. Fan, X. Zhang, Q. Zan, W. Dong, S. Shuang, C. Dong, A red-emission  
459 fluorescent probe for visual monitoring of lysosomal pH changes during mitophagy and cell  
460 apoptosis, *Analyst.* 145 (21) (2020) 7018-7024.

461 [39] S. Biswas, T. Dutta, A. Silswal, R. Bhowal, D. Chopra, A.L. Koner, Strategic engineering of  
462 alkyl spacer length for a pH-tolerant lysosome marker and dual organelle localization, *Chem.*  
463 *Sci.* 12 (28) (2021) 9630-9644.

464